Spanish Journal of Agricultural Research
20 (4), e0208, 12 pages (2022)
eISSN: 2171-9292
https://doi.org/10.5424/sjar/2022204-19171
INIA-CSIC

RESEARCH ARTICLE

OPEN ACCESS

Novel draught resistance sensing elements for measurement of drawbar power of agricultural machinery

Ganesh Upadhyay[1], Hifjur Raheman[2] and Rashmi Dubey[3]

[1]Department of Farm Machinery and Power Engineering, College of Agricultural Engineering and Technology, CCS Haryana Agricultural University, Hisar, Haryana, 125004, India. [2]Department of Agricultural & Food Engineering, Indian Institute of Technology Kharagpur, West Bengal, 721302, India [3]School of Advanced Sciences, VIT AP University, Andhra Pradesh, 522237, India

Abstract

Aim of study: To develop an instrumentation system comprising three force sensing elements to measure the draught resistance of any tillage and seeding tools during field operation by connecting one sensing element to each three-point linkage of the tractor.

Area of study: Department of AgFE, Indian Institute of Technology, Kharagpur, India

Material and methods: Commercial S-type transducers were packed laterally in between the curved plates perpendicular to the direction of travel in such a way that the magnitude of the imposed force decreased and its nature got reversed consequently during tillage force measurement. Finite element analysis was also performed on the proposed model of the sensing elements. The performance was evaluated on the basis of non-linearity, hysteresis, and non-repeatability. The data were validated with the draught values simultaneously recorded using instrumented three-point linkages of tractor.

Main results: It offered good sensitivity and linearity during static calibration. The measurement capacity based on maximum applied load during static calibration was 10 kN with accuracy 93.40%. The low values of mean percentage error (9.03%), maximum absolute variation (17.43%), and root mean square error (0.51 kN) revealed good accuracy of the system. Validation was conducted by comparing the data for an offset type disk harrow with the model outputs of previous studies to assess its suitability for other soil working conditions, and the results were satisfactory.

Research highlights: The advantages of this sensing device in the measurement of drawbar power are fewer changes in the hitching geometry, lower cost, and capability of quick hitching.

Additional keywords: three-point linkage; database generation; Wheatstone bridge; finite element method

Abbreviations used: CI (cone index); DSS (decision support systems); EORT (extended octagonal ring transducer); FEM (finite element method); MAD (maximum absolute deviation); MAPD (mean absolute percentage deviation); PTO (power take-off); RMSD (root mean square deviation).

Citation: Upadhyay, G; Raheman, H; Dubey, R (2022). Novel draught resistance sensing elements for measurement of drawbar power of agricultural machinery. Spanish Journal of Agricultural Research, Volume 20, Issue 4, e0208. https://doi.org/10.5424/sjar/2022204-19171

Received: 12 Jan 2022. **Accepted**: 03 Oct 2022.

Funding agencies/institutions: Ministry of Human Resource Development (MHRD), Govt. of India.

Competing interests: The authors have declared that no competing interests exist.

Correspondence should be addressed to Ganesh Upadhyay: ganesh.upadhyay0@hau.ac.in

Introduction

The draught resistance is described as the force needed to propel machinery in the direction of motion (ASAE Standards EP291.3, 2005). The knowledge of draught resistance is often utilized in implement management to predict the power demand during tillage and sowing operations. Agricultural machinery consultants use the draught and energy data for suitable matching of tractors and implements and also to predict their fuel energy consumption. Farm management models utilize these data to choose suitable machinery by simulating and comparing the per-

formance with traditional agricultural systems. Precise knowledge of the draught resistance is required to develop reasonable models (Harrigan & Rotz, 1995). There have been three main approaches to estimate the draught resistance of any tillage machinery at varying soil and working conditions: 1) analytical, 2) empirical, and 3) numerical methods. Determination of draught force through analytical approaches (Kuczewski & Piotrowska, 1998; Godwin *et al*., 2007), mostly originated from the passive earth pressure theory, is less accurate compared to the empirical approach because of the non-homogeneity of soil structure and texture in the field. The empirical approaches (McKibben & Reed, 1952; Gee-Clough *et al*., 1978; Nicholson *et al*., 1984; Upadhyaya *et al*., 1985; Bashford *et al*., 1991; Grisso *et al*., 1996; Kheiralla *et al*., 2004) are based on the measurement of draught force in both laboratory and field at different soil, implement and working conditions. The recorded data are then examined by several statistical methods to develop a best-fit regression model for further selection and matching of implements. Numerical methods involve advanced computer software's using the finite element method (Kushwaha & Shen, 1995; Mouazen & Nemenyi, 1999; Bentaher *et al*., 2013), or discrete element modelling (Sadek & Chen, 2015). Several methods were followed in the past to determine the draught of tillage implements. This included spring, hydraulic, and strain gage type dynamometers, and three-point hitch dynamometers with suitable data acquisition systems to gather the draught data in both laboratory and field studies. Sarkar *et al*. (2021) and Choudhary *et al*. (2021) suggested that more analytical studies and alternative approaches are required to measure and predict the energy requirements of tillage implements, to help in proper matching, and to develop decision support systems (DSS).

A precise understanding of the tractor linkage geometry is needed for the design of load sensing components in the linkages to estimate the magnitude of draught resistance. The drawbar power of trailed implements is generally measured by a hydraulic, spring, or strain gauge type dynamometer. The mounted type implements necessitate the use of a three-point linkage dynamometer to quantify the soil resistance contributing toward drawbar power (Chung *et al*., 1983; Al-jalil *et al*., 2001; Kepner *et al*., 2005). However, many of these dynamometers are suitable specifically for a particular tractor-implement combination and not easily adaptable to others. The various three-point linkage dynamometers were either installed on a fabricated structure between the tractor and machinery or attached integrally with modifications in the dynamometer arms to incorporate the necessary sensors. The frame type three-point linkage dynamometers are fabricated to suit different category tractor hitches. However, attaching and detaching these heavy and rigid frame structures with the implements is cumbersome and require quick coupling arrangements. Also, fixing them on the three-point hitch alters the mast height and lower hitch point spread which is not desirable as it ultimately affects the hitch forces, implement stability, operating depth, and line of pull.

Scholtz (1966) suggested that a dynamometer should be able to fit on multiple implements without requiring any alteration in the implement hitch geometry. It should not obstruct the use of a power take-off (PTO) shaft and should require a minimum number of measuring channels. Palmer (1992) developed a dynamometer configured as a quick hitch arrangement suitable for categories I, II, or III tractors using commercial load cells. The dynamometer was suitable to measure horizontal, vertical, and lateral forces, and their respective moments. However, its heavy weight (about 350 kg) and rearward shifting of the machinery by 17.35 cm limited its applicability to low horsepower tractors and lighter-weight machinery. Chaplin *et al*. (1987) constructed a three-point hitch dynamometer with a precision of 5% while measuring the draught up to 45 kN. Upadhyay & Raheman (2018) measured the draught force in a soil bin with the help of a S-type force transducer mounted horizontally between the soil processing trolley and intermediate trolley. Kumar *et al*. (2016) and Upadhyay & Raheman (2019a) used a mechatronic device to measure draught and wheel slip. The developed dynamometer was in the form of a detachable frame with force transducers accommodated in the sensing elements within the frame to sense and measure the draught of the implement.

The extended octagonal ring transducer (EORT) was used by several investigators to analyze different forces and moments that act on tractor three-point linkages and PTO bearing (Thakur & Godwin, 1988; Watyotha & Salokhe, 2001; Hensh *et al*., 2021a). However, precise identification of stress node locations for positioning and fixing the strain gauges is crucial and requires preliminary experiments or software simulations as it otherwise affects the cross-sensitivity. Also, the installation of strain gauges is complex and requires good knowledge and preciseness. Godwin *et al*. (1993) developed a system employing EORTs fixed perpendicularly to measure the orthogonal forces and moments to a maximum of 100 kN and 100 kN-m, respectively. O'Dogherty (1996) developed a suitable procedure in terms of geometrical parameters for designing the EORT. He also derived a design model to calculate the appropriate ring thickness of EORT. Agrawal & Thomas (2003) used eight strain gages in the form of two Wheatstone bridges mounted on the two rings of an EORT made of mild steel for measuring horizontal and vertical forces acting on a mouldboard plough. Al-Janobi (2000) developed a data recording system equipped with EORTs for the two lower links along with a load cell for the top link. Chen *et al*. (2007) measured the performance of a double EORT drawbar dynamometer having a draught range of 180 kN developed for the measurement of drawbar power for a sweep-type manure injector. Optimal strain-gage positions were located with the help of the finite element method (FEM) to reduce cross-sensitivity among acting forces.

The objective of this research was to test the potential of using a novel low-cost technique for the estimation of draught resistance of any tillage and seeding tools during field operations. Design criteria such as ease of construction, suitability for different types and sizes of implements having varying hitch point spread and mast height without alterations, and quick hitch capability were also taken into account.

Material and methods

Development of draught measurement device

The forces acting on a tractor during field operation play a crucial role in the energy requirement, traction mechanics, stability analysis, and steering control. Three force sensing elements (Fig. 1a) were constructed to measure the draught resistance of agricultural machinery by mounting them to the left, right, and top hitching points. Each sensing element comprised two detachable MS frames (1, 2) and two curved plates (3) with the provision of fixing a commercial S-type force transducer (4). One frame of the sensing element was connected with the tractor linkage (1) while another was connected with the implement hitch (2). Each S-type force transducer had a range and least count of 5000 N and 0.05 kg, respectively for sensing and measuring the forces on a particular linkage. The transducers were packed laterally in between the curved plates perpendicular to the direction of travel in such a way that the magnitude of the imposed force decreased and its nature got reversed consequently at the time of tillage force measurement. When tensile force acted on the sensing element, the curved plates tried to extend, which ultimately imposed compressive force on the force transducer, as also presented in Fig. 1b. Similarly, when the force of compressive nature acted on the sensing element, the curved plates tried to flex and imposed tensile force on the force transducer.

The draught resistance is described as the force needed to drive machinery in the direction of motion (ASAE Standards EP291.3, 2005). The arrangement of fixing the draught sensing elements permits only resultant horizontal force components to act on the force transducer. Thus, the draught was straightaway predicted by deducting the force acting on the top sensing element from the summation of forces acting on lower sensing elements (Eq. 1). The forces measured during the field experiments were acquired for further analysis through a portable DAQ system powered using the tractor battery.

$$D_f = F_R + F_L - F_T \quad (1)$$

where, D_f is the draught resistance, kN; F_R, F_L, and F_T are measured forces in kN in the right, left, and top link sensing elements, respectively.

a)

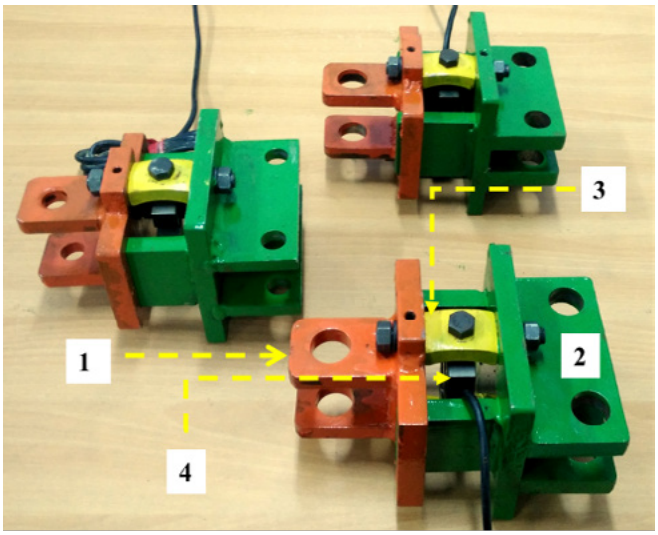

b)

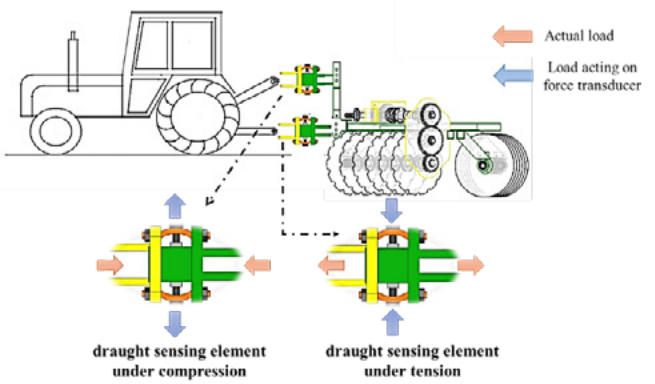

Figure 1. Position of mounting the draught sensing elements along with force representation: a) developed draught sensing elements; b) force representation on the draught sensing elements. 1. Tractor side frame. 2. Implement side frame. 3. Curved plate. 4. S-type force transducer

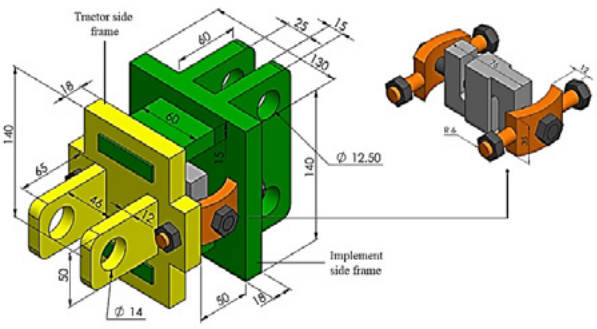

Figure 2. Isometric drawing of one draught sensing element with specific dimensions (all dimensions are in mm).

The isometric view of the developed draught sensing element with detailed dimensions is shown in Fig. 2. The weight of each developed draught element was 7.5 kg.

Finite element (FE) simulation of the proposed draught sensing elements

Finite element (FE) analysis was performed in ANSYS R15.0 workbench on the designed 3D model of the draught sensing element to check whether its design is safe or not. The prototype model is generally considered to be safe in the static structural analysis if the induced equivalent stress and deformation of components are less than the allowable stress and deformation of the selected material (Karmakar & Kushwaha, 2006; Bentaher *et al*., 2013; Upadhyay *et al*., 2017). The results on induced von Mises stresses and deformations were examined, and consequently, the required modifications were made in the 3D design prototype for obtaining optimum components dimensions before the development. The applied forces and boundary constraints on one lower link draught sensing element are shown in Fig. 3a. A horizontal force of 15000 N was applied on the tractor side frame of the draught sensing element (indicated as B), and the implement side frame was fixed (indicated as A). The results of FE analysis are presented in Figs. 3b and 3c in the form of coloured contours indicating degrees of stresses and deformations induced in the prototype. The maximum equivalent stress induced (129.84 MPa) was found to be lower compared to the yield strength of the material (mild steel having a yield strength of 250 MPa) indicating the design of draught sensing elements to be safe.

a)

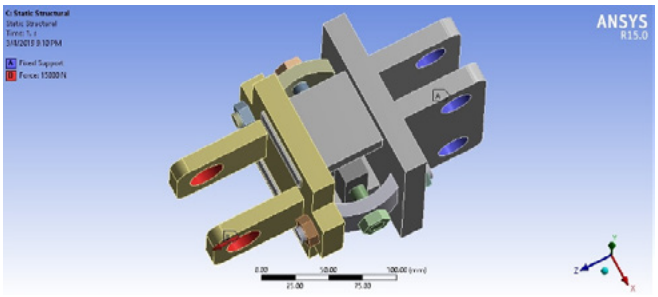

b)

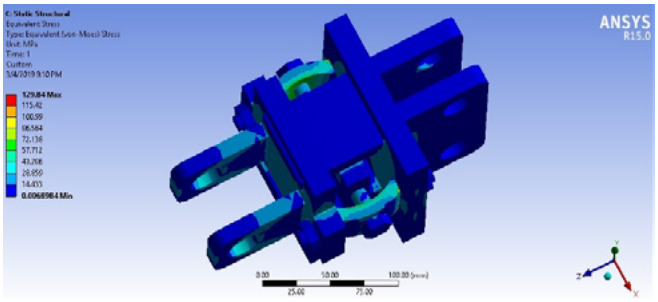

c)

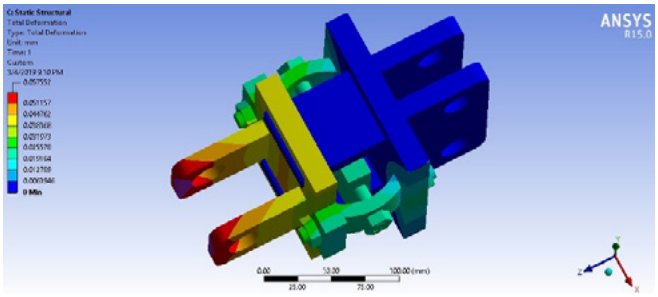

Figure 3. Results of finite element (FE) analysis for the draught sensing unit: a) applied forces and boundary conditions on the lower link draught sensing unit; b) equivalent von Mises stresses induced; c) total deformation.

a)

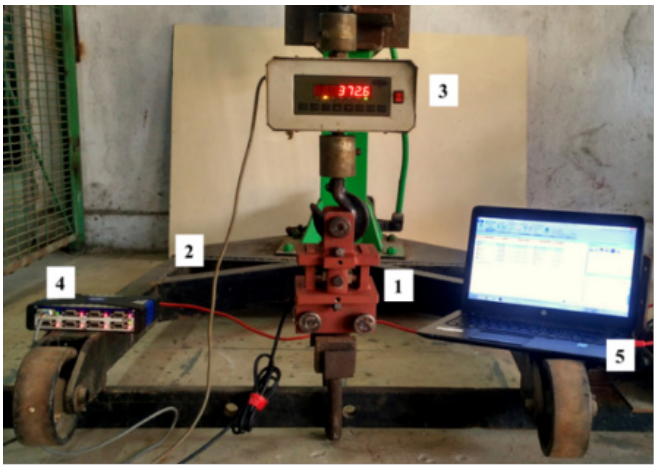

b)

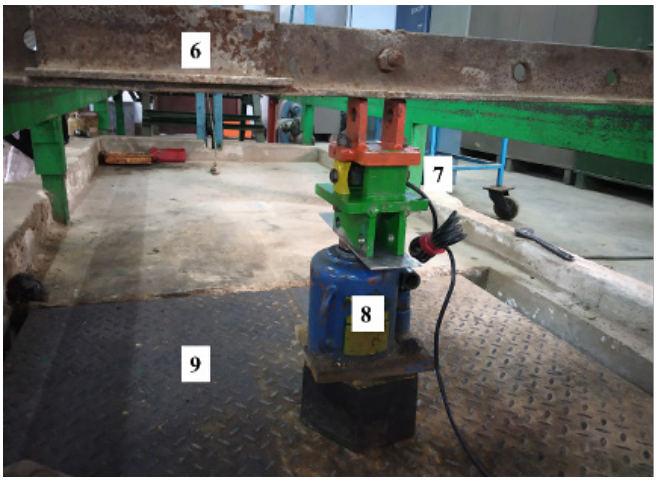

Figure 4. Calibration setups for draught sensing elements: a) Lower linkage sensing element under tension; b) Top linkage sensing element under compression. 1. Sensing element. 2. Mechanical crane. 3. Certified digital weighing balance. 4. Data logging system. 5. Personal laptop. 6. Fixed bar. 7. Load cell. 8. Hydraulic jack. 9. Weighing platform.

Laboratory calibration of the draught sensing elements

The dynamometer elements which were fixed to the left and right linkages of the tractor were calibrated under tensile conditions using a mechanical floor crane. The calibration setup used is shown in Fig. 4a. One end of the sensing element was clamped to the bolt of the crane at the bottom, and another end was connected to the crane pulley hook through a certified weighing balance with a digital display having 1000 kg capacity and 0.1 kg least count. The elements were gradually loaded with ratchet pinion of the loading crane from 0 to 900 kg in steps of 50 kg and the resulting force coming on the load cell was logged using an HBM Quantum-X DAQ system.

The top link sensing element was calibrated under compression. The calibration setup (Fig. 4b) consisted of a hydraulic jack placed on a weighing platform. The top link sensing element was mounted between the hydraulic jack and a fixed iron bar. Known force on the element was applied using the hydraulic jack. Because of the fixed bar at the top, the same load was getting transmitted to the weighing platform, and the readings of the force exerted on the weighing platform were displayed on the digital weighing balance.

Development of instrumented three-point linkages of tractor for validation of the developed draught sensing elements

To validate the developed draught sensing elements, a system comprising instrumented three-point linkage was also developed (Fig. 5), consisting of strain gauges in Wheatstone bridge arrangement for simultaneous determination of draught in the field (Upadhyaya *et al*., 1985; Sahu, 2005; Roul, 2014; Upadhyay, 2020). The electrical strain gauges (320 Ω, gauge factor 2.6) were fixed on lower linkages to determine the tension and bending. A circular proving ring was fixed on the top linkage to assess the compression. Three rotary position sensors helped to determine the angles of lower linkages in the horizontal and vertical planes, and the angle of the top linkage in the vertical plane.

To determine the lower linkage forces under tension, four active gauges (T1, T2, T3, and T4) were installed on the imaginary neutral axis. For neglecting the effect of temperature, four dummy gauges (D1, D2, D3, and D4) were fixed on a separate metal piece. The arrangement of strain gauges on the lower linkages is given in Fig. 6a. Active gauges were configured such that they were only responsive to tension and irresponsive to bending. Lateral force compensation was accomplished by arranging T1 and T3 gauges opposite to T2 and T4. With these gauges, a Wheatstone bridge circuit (Fig. 6b) was configured to measure the tensile force.

For determining the bending in lower linkages, eight active strain gauges (B1, B2, B3, B4, B1', B2', B3', and B4') were installed on the upper and lower faces of the lower links (Fig. 6a). The gauges B2, B4, B2', and B4' were installed between the implement hitch point and the lifting rod; and B1, B3, B1', and B3' were installed behind the lifting rod. Bending causes tension in B1, B1', B2, and B2' and compression in B3, B3', B4, and B4'. Since all the eight gauges were strained to the same amount when subjected to a tensile force; the output of the Wheatstone bridge circuit was not affected due to a tensile force. Thus, all active gauges were sensitive to bending force only. Utilizing these gauges, a circuit (Fig. 6b) was configured to measure the bending force.

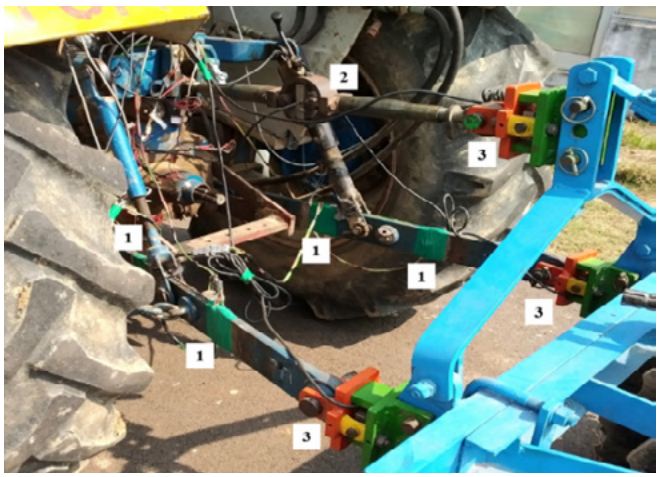

Figure 5. Instrumented three-point linkages to validate the developed draught sensing elements. 1. Strain gauges positions. 2. Top linkage proving ring. 3. Draught sensing elements.

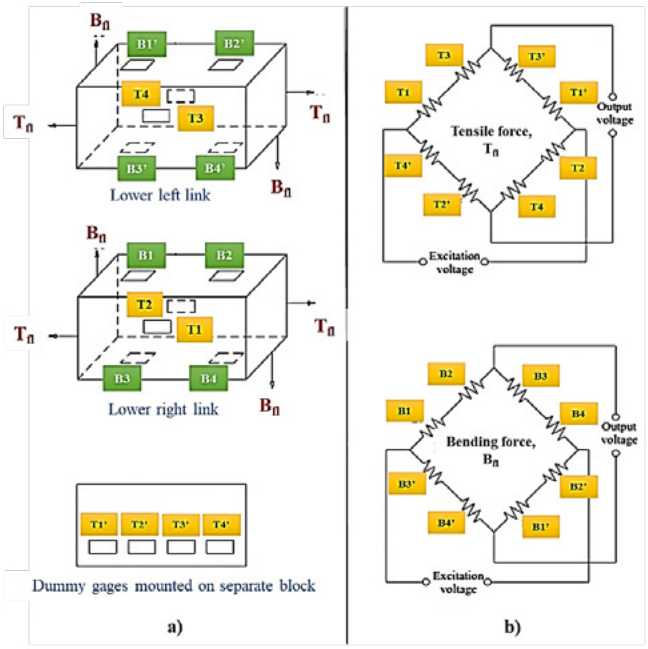

Figure 6. Arrangements of strain gages and circuit diagrams for measuring lower linkage forces: a) configuration of strain gauges. b) Wheatstone bridge circuit.

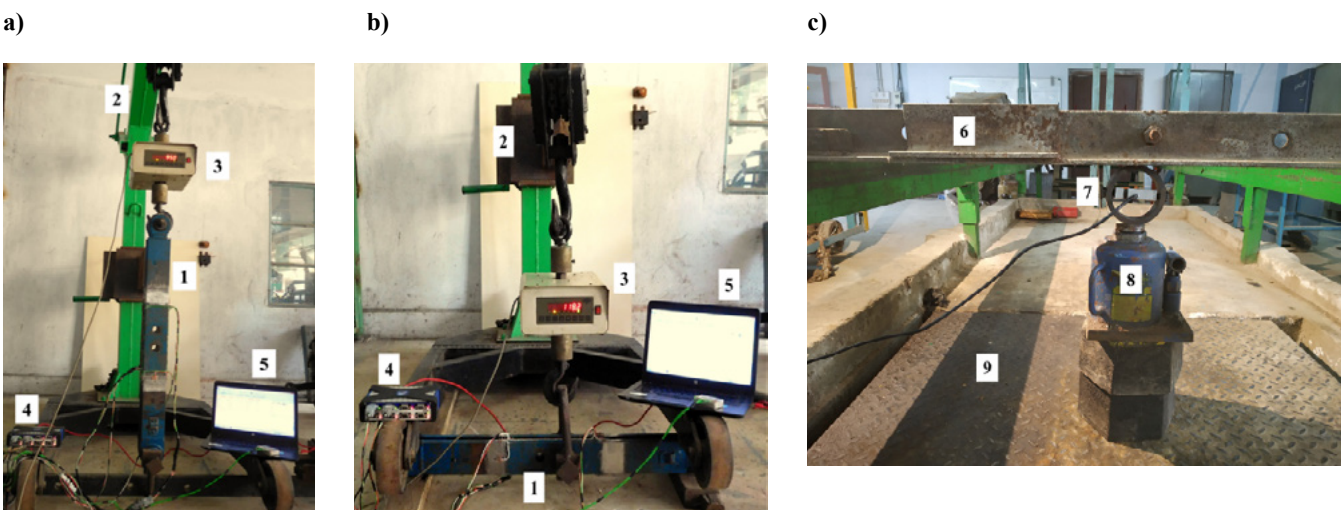

Figure 7. Calibration set up for different linkages of the tractor: a) tensile force in lower linkage; b) bending force in lower linkages; c) compressive force in top linkage. 1. Lower links. 2. Mechanical floor crane. 3. Certified digital weighing balance. 4. Data logging system. 5. Personal laptop. 6. Fixed bar. 7. Proving ring. 8. Hydraulic jack. 9. Weighing platform.

To measure the force on the top linkage, mild steel proving circular ring was fitted at the position of the turnbuckle. The ring was fabricated as per the standard design methodology (Godwin *et al*., 1993; O'Dogherty, 1996). A S-type force transducer having 1000 kg range was fitted inside the proving ring such that the compressive stress in the top linkage induced tension in the force transducer and vice versa.

Calibrations of the instrumented three-point links were carried out under both tension and bending for lower linkages and under tension for top linkage. For calibrating under tension, the lower linkages were held vertically by fixing one side of the linkage and attaching the other side to the hook of the crane with a certified digital weighing balance in-between having 1000 kg capacity and 0.1 kg least count (Fig. 7a). For calibrating under bending, the lower linkages were placed horizontally under the base frame of the mechanical crane. The end sections of both the lower linkages were held together and the load was applied at the centre position (Fig. 7b). For each calibration, the linkages were loaded up to 900 kg with step load increments of 50 kg, and the respective bridge outputs were logged using a data acquisition (DAQ) system. For calibration of the top linkage, a compressive load was applied on the proving ring from 0 to 950 kg in steps of 50 kg following the similar procedure as used for calibration of the top link draught sensing element (Fig. 7c). The bridge output of the force transducer was logged using a DAQ system.

A 10k ohms rotary position sensor was mounted on a fabricated frame attached to the tractor above PTO for determining the vertical inclination of the top linkage. Besides this, two other rotary position sensors each of 10k ohms were used for measuring the vertical and horizontal inclinations of the lower link. Out of these rotary position sensors, one was fixed on the rocker arm of the tractor hydraulic system to assess the vertical inclination of the lower link, and the other one was fixed on the fabricated frames attached to the tractor on one side of PTO to gage the horizontal angle made by the lower link. The knobs of the position sensors rotated freely with the actuation of the three-point linkage. Calibrations of the rotary position sensors were conducted using a digital protractor. Bridge outputs with respect to different linkage angles were logged using the DAQ system.

Knowing the magnitude of forces acting on both lower links, top link, and the angles made by these links in horizontal and vertical planes, the draught of the implement was computed using the following expression (Eq. 2) according to the vector geometry (Upadhyaya *et al*., 1985; Sahu, 2005; Kumar *et al*., 2016; Upadhyay, 2020):

$$D_r = T_{fl} \cos\alpha \cos\beta + B_{fl} \cos\alpha \sin\beta - C_{ft} \cos\theta \cos\phi \qquad (2)$$

where, D_r is the draught resistance; T_{fl} and B_{fl} are the tension and bending forces in lower linkages; C_{ft} is the compression force in top linkage; α and β are the angles of lower linkages in the horizontal and vertical plane; θ and ϕ are the angles of top linkage in the horizontal and vertical plane.

Validation procedure for the field tests

The validation tests were conducted with a 46 horsepower 2WD tractor having a rated engine speed of 2500 rpm. The soil type was sandy clay loam (57.1% sand, 19.9% silt, and 23.0% clay) with soil water content, cone index (CI), and bulk density of the upper 120 mm layer varying in the range of 10.50-12.13% (db), 546-975 kPa, and 1420-1680 kg m^{-3}, respectively. The speed of the tractor engine was adjusted by the hand throttle before initiating each experimental run. Proper tyre pressures were maintained in the front

and rear wheels. The standard oven-drying technique (IS: 2720, 1973) was used for determining the soil water content under which the test samples have to be put in an oven for 24 hours at 105 ºC. The core cutter technique (IS: 2720, 1975) was followed for the measurement of the soil bulk density. The soil penetration resistance was determined using a sensor-based hydraulic cone penetrometer device designed by Upadhyay & Raheman (2020) having cone base and rod dimensions as per ASABE Standards S313.3 (2001). The depth of operation was determined by recording the distance between furrow sole and ground level along the furrow wall at an interval of about 5 m along the length of the test run and at least three locations along the width of cut of the implement. The loose soil was removed carefully up to the firm furrow sole before taking measurement. Hall effect sensors were installed on the front and rear tyres to determine the forward speed of operation following the procedures of Rasool *et al*. (2017) and Nataraj *et al*. (2021).

For performing experimental validation in the test plots, data on draught were measured simultaneously using both developed draught sensing elements and instrumented three-point links by varying tillage depth and forward speed between 80-120 mm and 3.50-7.00 km h^{-1}, respectively. The implement used was a mounted offset type disk harrow equipped with six cut-away concave disks mounted on the front arbor bolt and six plain concave disks at the rear. Each of the disks used had an outer circle radius of 28 cm, thickness of 0.4 cm, and centre concavity of 7 cm. Each cut-away disk had eleven notches (width 8.2 cm and depth 3.2 cm) at equal intervals. The data from both draught measurement systems were taken at 50 Hz set frequency in each channel of the HBM Quantum-X logging system (Darmstadt, Germany). Each trial was performed for a straight test run of 50 m without using the foot accelerator. The statistical investigation was accomplished in SPSS software.

The statistical indices considered for validation were: mean absolute percentage deviation (MAPD), root mean square deviation (RMSD), and maximum absolute deviation (MAD) (Upadhyay & Raheman, 2019b; Nataraj *et al*., 2021). MAPD was calculated for comparing the draught resistance accuracy of the measurement system in percentage. RMSD denotes the measurement capacity of the developed draught sensing elements in terms of residuals standard deviation. MAD helped to assess the maximum variation in draught resistance values measured with the sensing elements and the instrumented three-point linkages of the tractor.

Results and discussion

Calibration results of the developed draught sensing elements

The obtained calibration curves of draught sensing elements for left, right, and top linkages are given in Figs. 8a, 8b, and 8c respectively. The calibration results showed that the observed load varied linearly with the applied load with a good coefficient of determination (R^2) value of 0.99 for all the linkages. The sensitivity of the developed elements was measured to be 0.0889, 0.0812, and 0.1023 kg kg^{-1} of applied load for the left link (tensile force), right link (tensile force), and top link (compressive force), respectively. The draught measurement capacity of the sensing elements based on the maximum applied load during static calibration was 10 kN. The results of the analysis of variance indicated that the applied load significantly affected ($p \leq 0.01$) the measured output load. Further, the effect of loading and unloading on measured output was observed to be insignificant indicating no hysteresis effect.

Linearity, hysteresis, repeatability, and accuracy of the developed draught sensing elements

The performance of the draught sensing elements was evaluated based on accuracy, non-linearity, hysteresis, and non-repeatability. Separate tests were conducted with the same experimental setup in the loading mode to find the measurement accuracy of the developed sensor, which is defined as the maximum difference that existed between the draught measured using the developed sensing elements and the draught data simultaneously recorded using instrumented three-point linkages of the tractor. The experimental results showed that the measurement accuracy of the developed system was 93.40%, and the maximum error in the measured value was 0.66 kN.

Non-linearity is generally defined as the degree of offset by which the actual measured curve of a sensor departs from the ideal regression curve (Fraden, 2010; McGrath & Scanaill, 2013; Liu *et al*., 2018). Non-linearity was determined from the calibration curves by dividing the maximum deviation by the error in observed output load with full-scale input; it was found to be 1.95%, 1.44%, and 1.63% for the left link (tensile force), right link (tensile force), and top link (compressive force), respectively. Hysteresis which indicates the degree of misalignment between the input and output with the loading and unloading modes was also determined (Liu *et al*., 2018). With the maximum offset values of 1.27, 1.21, and 1.72 kg, the hysteresis values were found to be 1.50%, 1.58%, and 1.75% for the left link (tensile force), right link (tensile force), and top link (compressive force), respectively.

Repeatability, which indicates the ability of a sensor to provide the same result under the same circumstances, was also assessed several times in the terms of non-repeatability following standard procedures (Liu *et al*., 2018; Anonymous, 2021; Hensh *et al*., 2021b). To estimate the non-repeatability, tests were performed at applied load values of 200, 400, 600, and 800 kg using the same calibration setup in loading mode, each replicated 10 times. The non-repeat-

ability in terms of standard deviation (percentage of full-scale deflection) was found to be 2.34 kg (0.23%), 2.41 kg (0.24%), and 1.90 kg (0.19%) for left link (tensile force), right link (tensile force), and top link (compressive force), respectively.

Validation of the developed draught sensing elements with the instrumented three-point linkages of the tractor

The draught resistance measured using the developed draught sensing elements was validated with the draught values simultaneously recorded using instrumented three-point linkages of the tractor. The results of validation of draught data under different operating settings are shown in Fig. 9a. The results of field testing indicated that the developed elements were capable of providing reliable draught results with reasonable accuracy. A good agreement was observed among the simultaneously measured draught values from the two measurement systems with the slope of the line of best fit and R^2 value as 0.90 and 0.93, respectively.

The low values of MAPD (9.03%), MAD (17.43%), and RMSD (0.51 kN) showed good accuracy of the draught sensing elements. The deviations were acceptable taking in consideration the errors that may incur during field data collection. The draught resistance values were also examined using independent sample t-tests, and no statistically significant difference was found between the two measurement systems at 5% confidence bound. This shows that the developed system incorporating sensors at hitching points can provide valid reliable data on draught resistance of agricultural machinery as one would expect from using other techniques of draught measurement.

Correlation of measured draught resistance with the outputs from Roul (2014) model

The draught measured using developed sensing elements was also corroborated by comparing the values with the output from models developed by previous researchers at different combinations of soil cone indices, operating speeds, and depths.

Roul (2014) customized the standardized draught prediction equation of ASABE (ASABE D497.5, 2006) for predicting draught of offset-type disk harrows by incorporating the cone index variable to increase its suitability for sandy clay loam soil. This author conducted laboratory tests with various scale models of offset type disk harrow with disk radius and spacing of 16.5 cm and 12.5 cm, respectively, and gang angles set at 20º. Their modified model is given below (Eq. 3):

$$D_r=[A\times CI+B\times v+C\times v^2]\ \ w\times T_d \qquad (3)$$

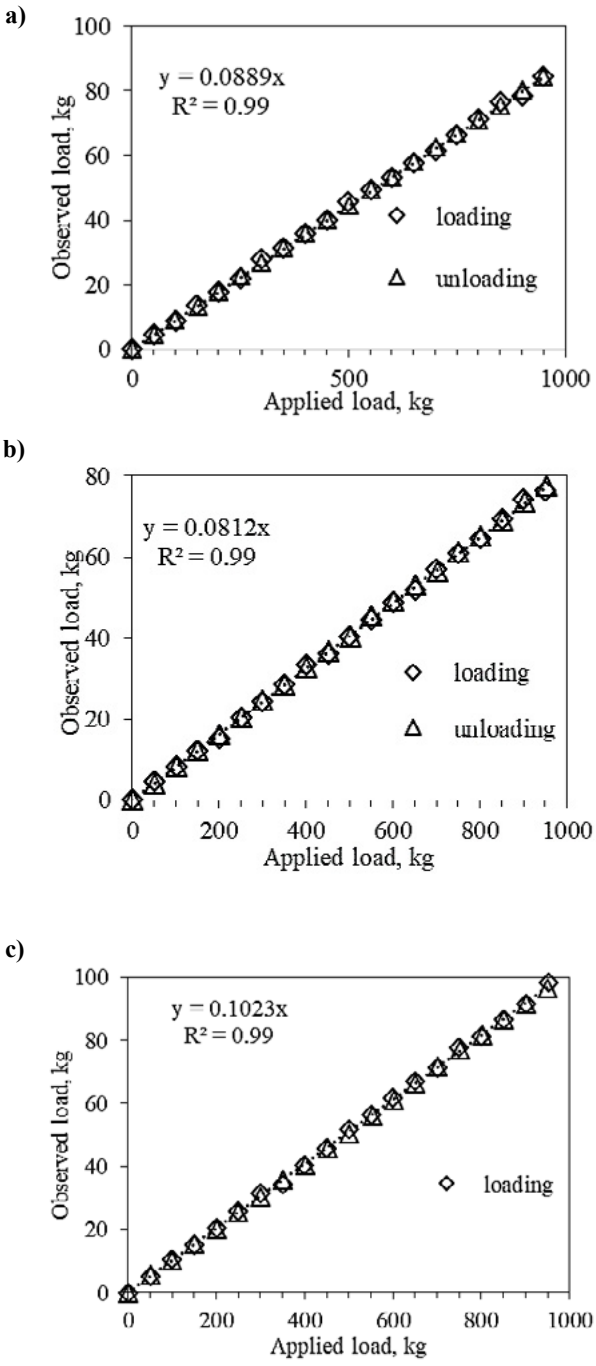

Figure 8. Calibration curves for draught sensing elements: a) Left link (tensile force); b) right link (tensile force); c) op link (compressive force).

where, D_r is the draught resistance in N; A, B, and C are the implement-related constants (A = 0.32, B = 37.96, and C = 0 for offset type disk harrow); CI is the soil penetration resistance in kPa; v is the operating speed in km h^{-1}; w is the width of operation in m; T_d is the tillage depth of operation in cm.

The estimated draughts determined from the Roul´s (2014) model and the corresponding draughts measured using the developed draught sensing elements are com-

pared in Fig. 9b by varying soil CI, operating speed, and tillage depth in the range of 500-1000 kPa, 3.5-7 km h^{-1}, and 80-120 mm, respectively. The average and maximum absolute deviations between the calculated draught resistance through Roul (2014) model and the draught measured using the developed system were observed to be 8.17% and 19.45%, respectively. The observed variation could be due to distinct specifications of the disks used in both studies and the errors experienced at the time of measurement tests. Fig. 9b shows that the slope of the best-fitted line is near one (m = 0.99) with good R^2 (0.91) which signifies that the draught sensing elements are able to measure the draught resistance in the field with good accuracy.

Correlation of measured draught resistance with the outputs from Upadhyay & Raheman (2019b) model

Upadhyay & Raheman (2019b) performed nonlinear regression analysis for the specific draught resistance of offset type disk harrow obtained during indoor soil bin investigations using Levenberg-Marquardt algorithm with suitable curve fitting technique. The soil type was sandy clay loam with a moisture content of 9-10% (db). They varied the front gang angle, tillage depth, operating speed and soil penetration resistance in the range of 25 to 40 degrees, 10 to 14 cm, 0.8 to 3.2 km h^{-1}, and 500 to 1100 kPa, respectively. Their proposed model (Eq. 4) is as follows:

$$D_{sp} = b_0 + b_1 \times \alpha + b_2 \times \alpha^2 + b_3 \times CI + b_4 \times v \qquad (4)$$

where, D_{sp} is the specific draught in kN m^{-2}, CI is the penetration resistance in MPa, v is the operating speed in km h^{-1}, α is the setting angle of front gang in degrees, b_i are the regression coefficients (b_0 = 75.04, b_1 = -4.97, b_2 = 0.07, b_3 = 30.31, b_4 = 6.67).

Specific draught values estimated from Eq. (4) were transformed into the draught resistance by multiplying them with the respective cross-sectional area of the furrow. The estimated draughts determined from this model and the corresponding draughts measured using the developed draught sensing elements are compared in Fig. 9c by varying soil CI, forward velocity, and tillage depth in the range of 500 to 1000 kPa, 3.5 to 7 km h^{-1}, and 80 to 120 mm, respectively. The value of α was 35º in our research. The average and maximum absolute variations between the estimated draught from Upadhyay & Raheman (2019b) model and the developed system were found to be 8.59% and 22.89%, respectively. The observed variation could be due to distinct specifications of the disks used in both studies and the errors experienced during measurement tests. The slope of the illustrated line (Fig. 9c) is close to one (m = 0.83) with a high R^2 of 0.92. These findings indicate that the draught sensing elements can measure the draught of agricultural implements with reasonable accuracy.

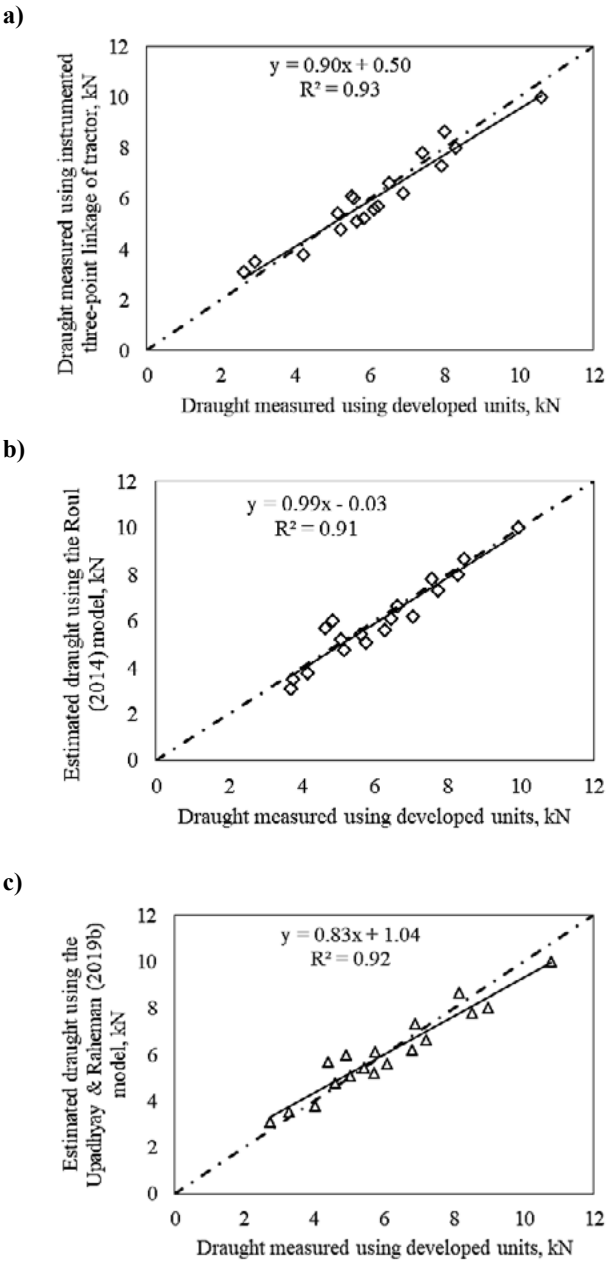

Figure 9. Correlation of measured draught resistance from developed sensing elements with outputs from: a) instrumented three-point linkage of tractor; b) Roul (2014) model; c) Upadhyay & Raheman (2019b) model.

The advantages of this sensing device is its ease of construction, least changes in the hitching geometry, lower cost, and capability of quick hitching. The distance between lower hitch points and mast height was not affected with the use of these developed elements. However, the implement shifted backward by 175 mm. The lower cost is due to the smaller capacity of load cells required because the force on the load cell comes through an indirect path through curved plates with reduced magnitude. These elements may be mounted on any type of agricultural tractor and machinery by just changing the design of the imple-

ment side frame according to the hitching arrangement of the implement used. Because of the separate use of sensing elements for all the hitching points, the different lower hitch point spread and the mast height provided in different implements are not a concern.

Conclusions

An instrumentation system involving three force sensing elements was designed to measure the draught resistance of any tillage and seeding tools during field operation. The draught measurement capacity of the sensing elements was 10 kN along with an accuracy of 93.40%. Non-linearity was observed to be 1.95%, 1.44%, and 1.63% for the left link (tensile force), right link (tensile force), and top link (compressive force), respectively. The hysteresis and non-repeatability were found to be 1.50% and 0.23%, 1.58% and 0.24%, and 1.75% and 0.19% for left, right, and top links, respectively.

A system involving instrumented three-point linkages was also developed and calibrated consisting of strain gauges in Wheatstone bridge arrangement for simultaneous measurement and validation of the draught in the field. The results of field testing indicated that the developed elements were capable of providing reliable draught results with reasonable accuracy. The draught measured using developed sensing elements was also corroborated by comparing the values with the output from models developed by previous researchers at different combinations of soil cone indices, operating speeds, and depths. The average and maximum absolute variations between the estimated draught from Roul (2014) model and the developed system were observed to be 8.17% and 19.45%, respectively. The corresponding variations between Upadhyay & Raheman (2019b) model and the developed system were found to be 8.59% and 22.89%, respectively.

The developed instrumentation system is simple, reliable, and could be useful in database generation, implement design, and matching for effective utilization of tractor engine power. The uniqueness of this sensing device is its ease of construction, least changes in the hitching geometry, lower cost, and capability of quick hitching. Because of the separate use of sensing elements for all the hitching points, the different lower hitch point spread and the mast height provided in different implements are not a concern.

Authors' contributions

Conceptualization: G. Upadhyay, H. Raheman.
Data curation: G. Upadhyay, H. Raheman, R. Dubey.
Formal analysis: R. Dubey.
Funding acquisition: H. Raheman.
Investigation: G. Upadhyay, H. Raheman.
Methodology: G. Upadhyay.
Project administration: H. Raheman.
Resources: H. Raheman.
Software: R. Dubey.
Supervision: G. Upadhyay, H. Raheman.
Validation: G. Upadhyay, H. Raheman.
Visualization: G. Upadhyay, H. Raheman.
Writing – original draft: G. Upadhyay.
Writing – review & editing: G. Upadhyay, R. Dubey.

References

Agrawal KN, Thomas EV, 2003. Relationship of specific draft with soil and operating parameters for M. B. plough. AMA 34(2): 9-12.

Al-Jalil HF, Khdair A, Muahal W, 2001. Design and performance of an adjustable three-point hitch dynamometer. Soil Till Res 62(1): 153-156. https://doi.org/10.1016/S0167-1987(01)00219-7

Al-Janobi A, 2000. A data-acquisition system to monitor performance of fully mounted implements. J Agric Eng Res 75(1): 167-175. https://doi.org/10.1006/jaer.1999.0496

Anonymous, 2021. How to perform a repeatability test for estimating uncertainty in measurement. https://www.isobudgets.com/how-to-perform-a-repeatability-test/ [Sept 2021).

ASABE Standards, 2001. Soil Cone Penetrometer. St. Joseph, MI, USA, ASAE S313.3.

ASABE Standards, 2006. Agricultural machinery management data. St. Joseph, MI, USA, ASAE D497.5.

ASAE Standards, 2005. Terminology and definitions for soil tillage and soil-tool relationships. St. Joseph, MI, USA, ASAE EP291.3.

Bashford LL, Byerly DV, Grisso RD, 1991. Draft and energy requirements of agricultural implements in semi-arid regions of Morocco. AMA 22(3): 79-82.

Bentaher H, Ibrahmi A, Hamza E, Hbaieb M, Kantchev G, Maalej A, Arnold W, 2013. Finite element simulation of moldboard-soil interaction. Soil Till Res 134: 11-16. https://doi.org/10.1016/j.still.2013.07.002

Chaplin J, Lueders M, Zhao Y, 1987. Three point hitch dynamometer design and calibration. Appl Eng Agric 3(1): 10-13. https://doi.org/10.13031/2013.26634

Chen Y, McLaughlin NB, Tessier S, 2007. Double extended octagonal ring (DEOR) drawbar dynamometer. Soil Till Res 93: 462-471. https://doi.org/10.1016/j.still.2006.06.008

Choudhary S, Upadhyay G, Patel B, Jain M, 2021. Energy requirements and tillage performance under different active tillage treatments in sandy loam soil. J Biosyst Eng 46(4): 353-364. https://doi.org/10.1007/s42853-021-00112-y

Chung YG, Marley SJ, Buchele WF, 1983. Development of a three-point dynamometer. Trans ASAE 22(2): 226-228.

Fraden J, 2010. Sensor characteristics. In: Handbook of modern sensors, Springer, NY, pp: 13-52. https://doi.org/10.1007/978-1-4419-6466-3_2

Gee-Clough D, McAllister M, Pearson G, Evernden DW, 1978. The empirical prediction of tractor-implement field performance. J Terra 15(2): 81- 94. https://doi.org/10.1016/0022-4898(78)90026-5

Godwin RJ, Reynolds AJ, O'Dogherty MJ, Al-Ghazal AA, 1993. A tri-axial dynamometer for force and moment measurements on tillage implements. J Agric Eng Res 55(3): 189-205. https://doi.org/10.1006/jaer.1993.1043

Godwin RJ, O'Dogherty MJ, Saunders C, Balafoutis AT, 2007. A force prediction model for mouldboard ploughs incorporating the effects of soil characteristic properties, plough geometric factors and ploughing speed. Biosyst Eng 97(1): 117-129. https://doi.org/10.1016/j.biosystemseng.2007.02.001

Grisso RD, Yasin M, Kocher MF, 1996. Tillage implement forces operating in silty clay loam. T ASAE 39(6): 1977-1982. https://doi.org/10.13031/2013.27699

Harrigan TM, Rotz CA, 1995. Draft relationships for tillage and seeding equipment. Appl Eng Agric 11(6): 773-783. https://doi.org/10.13031/2013.25801

Hensh S, Tewari VK, Upadhyay G, 2021a. An instrumentation system to measure the loads acting on the tractor PTO bearing during rotary tillage. J Terra 96: 1-10. https://doi.org/10.1016/j.jterra.2021.04.004

Hensh S, Tewari VK, Upadhyay G, 2021b. A novel wireless instrumentation system for measurement of PTO (power take-off) torque requirement during rotary tillage. Biosyst Eng 212: 241-251. https://doi.org/10.1016/j.biosystemseng.2021.10.015

IS: 2720, 1973. Method of test for soils, Part II: Determination of moisture content. Bureau of Indian Standards, Manak Bhavan, New Delhi.

IS: 2720, 1975. Method of test for soils, Part 29: Determination of dry density of soils in-place by the core-cutter method. Bureau of Indian Standards, New Delhi, India. Reaffirmed, 1-9.

Karmakar S, Kushwaha RL, 2006. Dynamic modeling of soil-tool interaction: an overview from a fluid flow perspective. J Terra 43(4): 411-425. https://doi.org/10.1016/j.jterra.2005.05.001

Kepner RA, Bainer R, Barger EL, 2005. Principles of farm machinery, 4th ed, Chapter 3. CBS Publishers, New Delhi.

Kheiralla AF, Yahya A, Zohadie M, Ishak W, 2004. Modelling of power and energy requirements for tillage implements operating in Serdang sandy clay loam, Malaysia. Soil Till Res 78: 21-34. https://doi.org/10.1016/j.still.2003.12.011

Kuczewski J, Piotrowska E, 1998. An improved model for forces on narrow soil cutting tines. Soil Till Res 46(3-4): 231-239. https://doi.org/10.1016/S0167-1987(98)00101-9

Kumar AA, Tewari VK, Nare B, 2016. Embedded digital draft force and wheel slip indicator for tillage research. Comput Electron Agric 127: 38-49. https://doi.org/10.1016/j.compag.2016.05.010

Kushwaha RL, Shen J, 1995. Numeric simulation of friction phenomenon at soil-tool interface. Tribol Trans 38(2): 424-430. https://doi.org/10.1080/10402009508983424

Liu Y, Tian T, Chen J, Wang F, Zhang D, 2018. A highly reliable embedded optical torque sensor based on flexure spring. Appl Bionics Biomech 2018: 1-14. https://doi.org/10.1155/2018/4362749

McGrath MJ, Scanaill CN, 2013. Sensing and sensor fundamentals. In: Sensor technologies, pp: 15-50. Apress, Berkeley, USA. https://doi.org/10.1007/978-1-4302-6014-1_2

McKibben EG, Reed IF, 1952. The influence of speed on the performance characteristics of implements. SAE Technical Paper. No. 520142. https://doi.org/10.4271/520142

Mouazen AM, Nemenyi M, 1999. Tillage tool design by the finite element method, Part 1. Finite element modelling of soil plastic behaviour. J Agric Eng Res 72(1): 37-51. https://doi.org/10.1006/jaer.1998.0343

Nataraj E, Sarkar P, Raheman H, Upadhyay G, 2021. Embedded digital display and warning system of velocity ratio and wheel slip for tractor operated active tillage implements. J Terra 97: 35-43. https://doi.org/10.1016/j.jterra.2021.06.003

Nicholson RI, Bashford LL, Mielke LN, 1984. Energy requirements for tillage from a reference implement. ASAE Paper No. 84-1028. St. Joseph, MI, USA.

O'Dogherty MJ, 1996. The design of octagonal ring dynamometer. J Agric Eng Res 63: 9-18. https://doi.org/10.1006/jaer.1996.0002

Palmer AL, 1992. Development of a three-point dynamometer for tillage research. J Agric Eng Res 52(3): 157-168. https://doi.org/10.1016/0021-8634(92)80057-Y

Rasool S, Raheman H, Upadhyay G, 2017. Development of an instrumentation system for evaluating the tractive performance of walking tractors. Int J Curr Microbiol Appl Sci 6(10): 759-770. https://doi.org/10.20546/ijcmas.2017.610.092

Roul AK, 2014. Draft prediction of commonly used tillage implements for sandy clay loam soil in India. PhD Thesis. IIT Kharagpur, Kharagpur, India.

Sadek MA, Chen Y, 2015. Feasibility of using PFC3D to simulate soil flow resulting from a simple soil-engaging tool. Trans ASABE 58(4): 987-996. https://doi.org/10.13031/trans.58.10900

Sahu RK, 2005. Development and performance evaluation of combination tillage implements for 2WD tractors. PhD Thesis. Agricultural and Food Engineering Department, IIT-Kharagpur, India.

Sarkar P, Upadhyay G, Raheman H, 2021. Active-passive and passive-passive configurations of combined till-

age implements for improved tillage and tractive performance: A review. Span J Agric Res 19(4): e02R01. https://doi.org/10.5424/sjar/2021194-18387

Scholtz DC, 1966. A three-point linkage dynamometer for restrained linkages. J Agric Eng Res 11(1): 33-37. https://doi.org/10.1016/S0021-8634(66)80006-9

Sheu PP, Chieng WH, Lee AC, 1996. Modeling and analysis of the intermediate shaft between two universal joints. J Vib Acoust 118: 88-99. https://doi.org/10.1115/1.2889640

Thakur TC, Godwin RJ, 1988. Design of extended octagonal ring dynamometer for rotary studies. AMA 19(3): 23-28.

Upadhyay G, 2020. Development and performance evaluation of a front active and rear passive set combined offset disc harrow. Doctoral dissertation, IIT Kharagpur.

Upadhyay G, Raheman H, 2018. Performance of combined offset disc harrow (front active and rear passive set configuration) in soil bin. J Terra 78: 27-37. https://doi.org/10.1016/j.jterra.2018.04.002

Upadhyay G, Raheman H, 2019a. Comparative analysis of tillage in sandy clay loam soil by free rolling and powered disc harrow. Eng Agric Environ Food 12(1): 118-125. https://doi.org/10.1016/j.eaef.2018.11.001

Upadhyay G, Raheman H, 2019b. Specific draft estimation model for offset disc harrows. Soil Till Res 191: 75-84. https://doi.org/10.1016/j.still.2019.03.021

Upadhyay G, Raheman H, 2020. Comparative assessment of energy requirement and tillage effectiveness of combined (active-passive) and conventional offset disc harrows. Biosyst Eng 198: 266-279. https://doi.org/10.1016/j.biosystemseng.2020.08.014

Upadhyay G, Raheman H, Rasool S, 2017. Three dimensional modelling and stress analysis of a powered single acting disc harrow using FEA. Curr Agric Res J 5(2): 203-219. https://doi.org/10.12944/CARJ.5.2.08

Upadhyaya SK, Kemble LJ, Collins NE, Camargo FA, 1985. Accuracy of mounted implement draft prediction using strain gauge mounted directly on three-point hitch linkage system. Trans ASAE 28(1): 40-46. https://doi.org/10.13031/2013.32199

Watyotha C, Salokhe VM, 2001. Development of a data acquisition system for measuring the characteristics of real time forces by cage wheels. J Terra 38: 201-210. https://doi.org/10.1016/S0022-4898(00)00021-5

Yang ZX, 2013. Oscillation in electric power steering test torque due to universal joint angle and control strategy. J Dyn Syst Meas Control 135(5): 051017. https://doi.org/10.1115/1.4024476